Facile Method for Fabricating Flexible Substrates with Embedded, Printed Silver Lines

Ankit Mahajan, Lorraine F. Francis,* and C. Daniel Frisbie*

Department of Chemical Engineering and Materials Science, University of Minnesota, Minneapolis, Minnesota 55455, United States

S *Supporting Information*

ABSTRACT: Insertion, curing and delamination is presented as a simple and scalable method for creating flexible substrates with embedded, printed silver lines. In a sequential process, aerosol-jet printed silver lines are transferred from a donor substrate to a thin reactive polymer that is directly adhered to a flexible substrate. Due to the unique ability of the aerosol jet to print continuous lines on a low energy surface, a 100% transfer of the printed electrodes is obtained, as confirmed by electrical measurements. Moreover, the root-mean-square roughness of the embedded electrodes is less than 10 nm, which is much lower than that for their as-printed form. The embedded electrodes are robust and do not show a significant degradation in electrical performance after thousands of bending cycles.

KEYWORDS: embedded silver lines, aerosol-jet printing, flexible epoxy coating, roll-to-roll manufacturing, printed electronics, flexible electronics
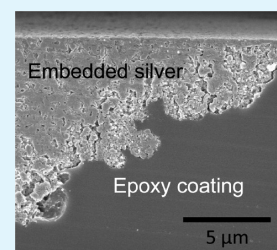
1. INTRODUCTION

The integration of electronic circuits into flexible and large area formats promises to deliver new functional capabilities that are difficult or expensive to achieve with traditional silicon-based electronics, such as bendable displays, foldable solar cells, large area sensors, flexible drug delivery patches and implants.[1−8] Central to continuous, high throughput flexible electronics manufacturing is printing, where an "ink" in the form of solution or suspension is deposited on a flexible substrate and dried to form a desired pattern. Printing of conductors, the most basic component of electronic circuits, is extensively reported in the literature.[9−14] For both superior current carrying capacity and high-density circuitry, conductors with large cross-sectional areas and high aspect ratios (thickness/width) are necessary.[15] Equally important is the uniformity and smoothness of printed conductor surfaces, because charge carriers are conveyed either across or along conductor interfaces in electronic devices.[16]

In organic thin film transistors (OTFTs), high-capacitance gate dielectrics, which are critical to low operating voltages, are generally achieved by coating an ultrathin polymer film or a self-assembled monolayer over a metal gate electrode.[17−20] Also, a composite electrode formed by coating a thin layer of a conductive polymer over a metal grid appears to be a strong candidate for substituting indium tin oxide as the transparent electrode in organic solar cells and light-emitting diodes.[21−23] Thus, many organic devices require overlaying a thin organic film on metal wires. Achieving a uniform coating on surfaces with topography is challenging, and coating defects can result in shorts, i.e., device failure. The problem is even more severe for printed conductors that have roughnesses of the same order as the thickness of the overlying film. From a manufacturing standpoint, topography on the substrate, courtesy of the printed electrodes, complicates the use of popular mass-production printing methods such as gravure or flexography, as these involve physical contact between the printing roll and the moving web. Furthermore, adhesion of printed metal tracks with plastic substrates is generally weak, necessitating an encapsulation layer for protection. For all of these reasons, developing methodologies for creating planarized flexible substrates with embedded, printed metallic tracks is essential.

Thermal imprinting has been used to create embedded silver meshes on plastic substrates.[24−26] In this technique, a flexible metallic master, wrapped around a heated roller, is pressed into a moving plastic substrate to form trenches. A silver ink is then filled into the trenches using a doctor blade. However, this method has several drawbacks, namely, a costly high-resolution metallic master, residue-covered land due to the doctor blade operation and nonflush silver because of thickness reduction from sintering. Another approach for obtaining embedded electrodes is transfer printing, where a polymer film is hot pressed over metallic features on a donor substrate and subsequently peeled off, resulting in transfer of features to the film.[27−30] However, a long holding time is potentially limiting for practical applications. A similar technique, template stripping, involves coating a polymer film over metal patterns deposited on a template surface, followed by a delamination step.[31−33] Recently, this technique has been employed for obtaining smooth silver nanowire films buried in a polymer matrix.[34−37] One main issue is that easy delamination requires thick polymer coatings, which limits the bendability of the embedded electrodes.[38,39] Also, to our knowledge, this technique has not been used for processing high resolution printed metal lines. Many high resolution printing methods,

e.g., inkjet, require merging of individual droplets on a high energy surface to form a continuous line. As a result, these lines also exhibit a strong adhesion with the substrate and therefore it is difficult to subsequently transfer them to another substrate for planarization.

Here, we report a simple method, called insertion, curing and delamination (ICD), for embedding high aspect ratio, printed silver lines into a thin polymer coating on a flexible substrate. ICD is based on the transfer of features from a donor to a receiving substrate but, unlike template stripping and transfer printing, consists of processing steps that are easily scalable for roll-to-roll (R2R) manufacturing. In particular, it employs low viscosity reactive liquids rather than thermoplastic melts, e.g., transfer printing, which facilitates rapid conformal contact with the donor substrate. Further, these reactive liquids are coated on high energy receiving substrates rather than low energy donor substrates, e.g., template stripping. This combination of features makes ICD compatible with thin coatings, a wide range of feature sizes, nonplanar surfaces and high speed (short contact time) R2R steps. The transfer yield is 100%, and the surface roughness of the embedded silver electrodes is less than 10 nm. The embedded electrodes exhibit excellent flexibility and robustness when subjected to mechanical stress, an essential requirement for truly flexible electronics.

2. EXPERIMENTAL SECTION

Printing of Silver Lines. All printing was accomplished using a commercially available aerosol jet printer (Optomec, Inc.). A commercial silver nanoparticle ink (UTDAg40X, UT Dots, Inc.), mixed with 10% v/v terpineol was used. The aerosol mist was generated by ultrasonication of 2 mL of the ink at 14 °C. The aerosol mist was transported to the print head outfitted with a 150 μm nozzle using a N_2 carrier gas. The ranges of flow rates of the carrier and sheath gas used were 18−25 and 40−60 sccm, respectively. Both focusing ratio (ratio of sheath gas flow rate to carrier gas flow rate) and stage speed were modulated to obtain silver lines with varied geometries.[15] A 125 μm thick silicone-coated polyethylene terephthalate (s-PET) film (8310 release coating, Saint-Gobain Performance Plastics, Ltd.) and a silane-treated silicon wafer were used as donor substrates. For silane treatment, the wafer was placed in a desiccator with 2 mL of trichloro(1H,1H,2H,2H-perfluorooctyl)silane (FOTS, Sigma Aldrich) solution. The desiccator was then pumped down to 1 Torr of pressure to allow the FOTS solution to evaporate. The sample was left overnight for complete coverage. The printed lines were sintered at 150 °C for 1 h in an atmospheric oven. s-PET was slowly cooled to room temperature and then inserted into the wet polymer coating. s-PET softened at 150 °C but restored its original stiffness upon slow cooling to room temperature.

Coating Preparation. For preparing the coating solution, the epoxy monomer and its curing agent (Epotek 310-M1) were thoroughly mixed in a 1.8:1 weight ratio, respectively, and vacuum degassed for 10 min. A wire wound rod was used to form a ~10 μm thick coating on a 75 μm thick polyimide film (Kapton, American Durafilm). Prior to coating, the substrate was cleaned with acetone, methanol, isopropyl alcohol and deionized water.

Insertion, Curing and Delamination. The printed substrate was inverted and slowly lowered onto the coated substrate at an angle approximately greater than 30° with the horizontal. Upon insertion of the silver features by gentle pressing, the coating was cured at 120 °C for 30 min on a hot plate. After complete cure, the top substrate was delaminated manually to obtain embedded silver lines in the epoxy coating.

Characterization of Embedded Lines. The embedded lines were imaged using a Hirox microscope (Digital Microscope KH-7700) and a scanning electron microscope (JEOL-6500). All atomic force microscopy (AFM) images were taken in the tapping mode on a Bruker Nanoscope IIIA atomic force microscope under ambient conditions. Resistance measurements were carried out using two Keithley 236 electrometers in a N_2-filled glovebox.

Bending Test. Mechanical bending of embedded electrodes was performed by attaching the substrate to a stationary block and a sliding stage, connected to computer-controlled positioning equipment (Aerotech Co.). The substrate was bent to a certain radius and restored to its initial state at a rate of 10 cm s^{-1} to complete one bending cycle. The "bending" radius was controlled by the displacement of the sliding stage. Electrical resistance of the electrodes was measured for every 2000 cycles for two different bending radii.

3. RESULTS AND DISCUSSION

The fabrication of embedded silver electrodes via ICD involves a series of steps, schematically illustrated in Figure 1. Initially, a
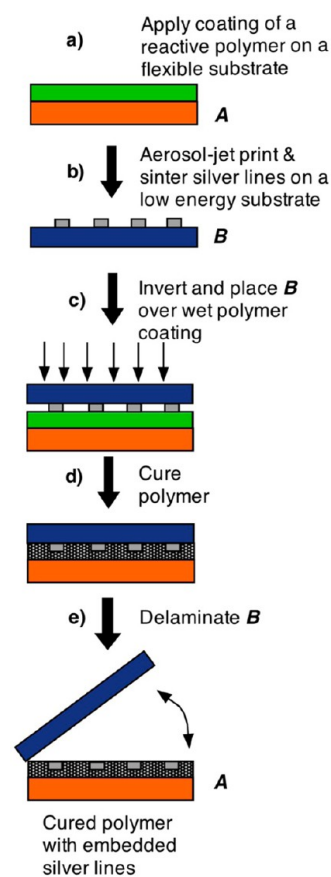

Figure 1. Scheme showing steps in insertion, curing and delamination (ICD). (a) A liquid prepolymer mixture of a reactive polymer is coated on a plastic substrate, A. (b) Silver patterns are aerosol-jet printed and sintered on a low energy flexible substrate, B. (c) B is inverted and lowered onto the wet polymer coating on A, ensuring complete insertion of the silver patterns and no air entrapment. (d) The prepolymer mixture is cured. (e) B is delaminated, leaving the silver patterns flush with the surface of the polymer coating on A.

thin (~10 μm) coating of a thermally cross-linkable, flexible epoxy prepolymer mixture is applied to a polyimide substrate. Silver electrodes are aerosol-jet printed and sintered on a different low surface energy, flexible substrate. Silicone-coated polyethylene terephthalate (s-PET) and silane-treated silicon were chosen for this work. This printed substrate is then inverted and lowered onto the prepolymer mixture at an angle that allows the liquid prepolymer to fill around the silver lines and air to escape. Subsequently, the prepolymer mixture, currently sandwiched between the two substrates, is thermally

cured forming a solid cross-linked film. Following complete cure, the top substrate is manually delaminated, leaving the silver patterns embedded in the epoxy coating.

The flushness of the silver line with the epoxy coating was verified using scanning electron microscopy (Figure 2). Figure
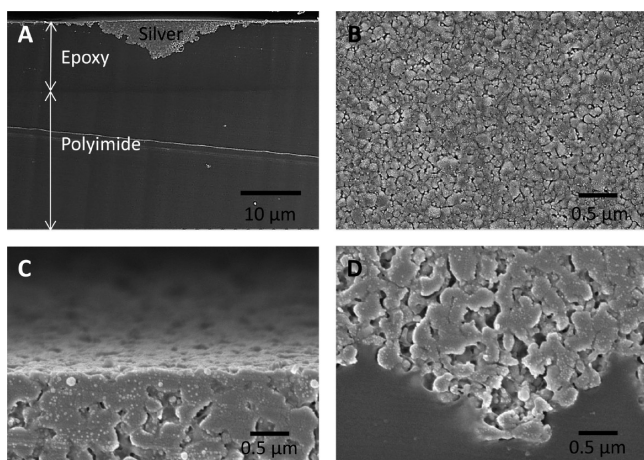

Figure 2. Scanning electron micrographs revealing (a) a silver line flush with an epoxy coating on a polyimide substrate, (b) surface topography of an embedded silver line, and extent of sintering of the silver nanoparticles near the (c) top and (d) bottom of the embedded line.

2a displays a cross-section scanning electron microscopy (SEM) image of a 40 μm wide, 6 μm tall (maximum height) silver line embedded in a 10 μm thick epoxy coating on a polyimide substrate. The embedded feature has a parabolic cross-section, which is typical of aerosol jet printed silver lines.[15] The flat, top surface of the silver metal flush with the polymer coating is clearly observed. Higher magnification images show uniform sintering across the cross-section of the lines (Figure 2c,d). The printed lines were annealed in an atmospheric oven, which provided uniform sintering conditions throughout the cross-section. Because of the low viscosity of the prepolymer mixture (~315 mPa·s), the epoxy prepolymer mixture could minutely track the footprint of the printed line, forming "microscopic fingers". As a result, the intrinsically fragile printed silver line is now firmly anchored by the polymer matrix.

An added advantage of ICD is the smoothness of the embedded features. Figure 2b displays the surface morphology of embedded silver, showing absence of any major topographical features. However, nanoscopic pores due to incomplete sintering of the silver nanoparticles are also apparent. The root-mean-square (rms) roughness characterized using AFM was 81.8 and 8.3 nm, respectively, for the as-printed and embedded silver, over a 25 μm^2 area (see Supporting Information, Figure S1a,b). Due to the low surface roughness, the embedded silver has a shiny, mirrorlike appearance, whereas the as-printed silver appears dull.

In ICD, the structure of printed silver is inverted such that the bottom surface comes to the top. Therefore, surface roughness of embedded silver depends on the "template" on which it is initially printed.[31] The rms roughness of our template, s-PET, over a 25 μm^2 area is found to be 1.80 nm (Supporting Information, Figure S1c). The flatness and smoothness of s-PET is transferred to silver, resulting in topography-free, smooth embedded features. However, the

presence of nanoscopic pores on the surface leads to a slight increase in its roughness compared to s-PET. The rms roughness of the revealed surface of the epoxy coating over a 25 μm^2 area is 1.83 nm, which matches well with the roughness of s-PET (Supporting Information, Figure S1d). Also, this surface is free from any residue from the delamination process, which makes it ideal for fabrication of electronic devices.

Central to ICD is the delamination step, where two important physical processes occur simultaneously. First, the interface between the donor substrate and the epoxy coating is cleaved, generating two new surfaces. The wettability of liquid prepolymer mixture on a substrate provides a good estimate of the interactions between the cured film and the substrate. The contact angles of the epoxy prepolymer mixture on s-PET and polyimide substrates were found to be 70.5° and 27.4°, respectively (Supporting Information, Figure S2). Quantitatively, the work of adhesion, W_A, of a liquid with a solid is expressed as

$$W_A = \sigma_L(1 + \cos\theta) \tag{1}$$

where σ_L is the surface tension of the liquid and θ is the contact angle of the liquid with the solid. Because of a lower value of W_A, s-PET could be delaminated from the cured epoxy coating by gentle peeling. On the other hand, owing to its strong adhesion with the epoxy, polyimide served as an excellent supporting film for the thin coating, forming a robust composite substrate. Despite the modulus mismatch, the thin epoxy coating was compliant to the underlying polyimide and the substrate showed no curling after the curing and delamination steps. Due to the strong adhesion, the substrate could be bent to radii as small as 1 mm without any noticeable delamination or other defects of the coating (Supporting Information, Figure S3).

The second process that occurs during delamination is the transfer of silver from the donor substrate to the epoxy coating. A high transfer yield requires a weak adhesion with the donor, which is possible with a low surface energy substrate. Both s-PET and silane-treated silicon qualify as low surface energy substrates, but printing continuous features on low energy surfaces is challenging due to ink dewetting.[40] We employed aerosol-jet printing (AJP) to overcome this problem. In AJP, a silver nanoparticle ink is atomized to generate an aerosol mist. The silver nanoparticles, entrained in the aerosol droplets, are transported by a flowing carrier gas to a print-head, where an annular sheath gas focuses the incoming stream, forming a high-speed jet. When the jet impinges a moving substrate, the aerosol droplets coalesce to form a liquid line. Due to the small (1−5 μm) size of the freshly generated aerosol droplets, rapid evaporation of solvent occurs during flight, leading to a significant increase in the solids loading and therefore viscosity of the aerosol droplets in the impinging jet. The high viscosity of the coalesced liquid diminishes the role of substrate's surface energy in determining the wetting characteristics and uniquely allows printing on a low energy surface.

Figure 3 demonstrates the versatility of ICD. Figure 3a shows the word "EMBEDDED" written using a combination of multioriented silver lines, buried in an epoxy coating using ICD, suggesting that the silver transfer is independent of orientation of the silver lines (with respect to the delamination direction). Due to the ease of the constituting steps in ICD, we could fabricate an embedded hexagonal grid of silver lines on a large area, flexible substrate (Figure 3b). To demonstrate the minimum feature size attainable using ICD, an array of 25
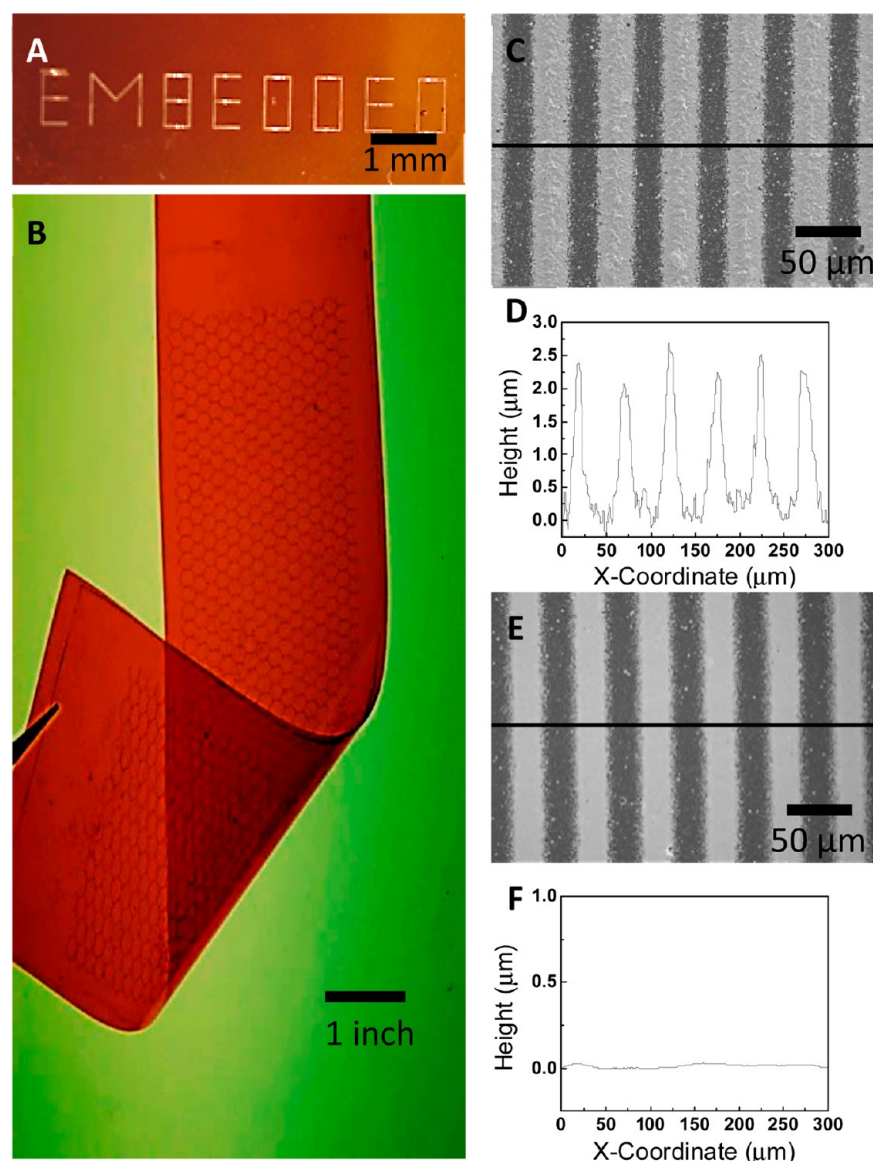
Figure 3. Versatility of ICD. (a) The letters "EMBEDDED" written using 50 μm wide silver lines, embedded in an epoxy-coated polyimide substrate. (b) An embedded hexagonal grid of 40 μm wide silver lines on a 10 in. long 3 in. wide substrate, demonstrating the scalability of ICD. (c) SEM image showing an array of silver lines (width, 25 μm; line spacing, 20 μm) on a silicone-coated PET donor substrate and (d) profilometric traces illustrating the cross section of the lines. (e) SEM image displaying the same lines upon embedment and (f) profilometric scan confirming the absence of topography on the substrate.

μm wide silver lines with a line-spacing of 20 μm was printed on s-PET and characterized using SEM and profilometry (Figure 3c,d). After embedding, the same lines appeared much smoother than their initial, as-printed form (Figure 3e) and were also completely flush with the surface of the epoxy (Figure 3f). As mentioned earlier, the low viscosity prepolymer mixture could easily fill the space between narrowly spaced lines, yielding a flat surface. Interestingly, even the tiny (0.1−0.5 μm) overspray clusters on either side of the lines, characteristic of AJP, were also transferred. It is worthwhile mentioning that the minimum feature size is not limited by any of the processing steps in ICD but depends on the resolution of the printing technique. ICD was found to be equally effective for complex patterns such as a 30 × 30 grid, fabricated using 20 μm wide silver lines with a 200 μm pitch (Supporting Information, Figure S4).

To measure the transfer yield, we investigated the change in electrical resistance of silver lines before and after ICD. Figure 4a shows the distribution of electrical resistance of 25 silver lines (each 5 mm long) printed and annealed on s-PET. Within error, no change is observed in the electrical resistance after embedding (Figure 4b), indicating 100% transfer. After delamination, the donor substrate was examined under an optical microscope and was completely free from silver residue. The same substrate was used multiple times without any substantial decrease in the transfer yield. We also found that the transfer yield did not vary much with different epoxy coating thicknesses, and the minimum coating thickness was limited by the thickness of the silver features.

To investigate mechanical flexibility and durability of the embedded electrodes, we examined the change in electrical resistance of five embedded electrodes subjected to repeated bending cycles at two different radii of curvature (r). Using a
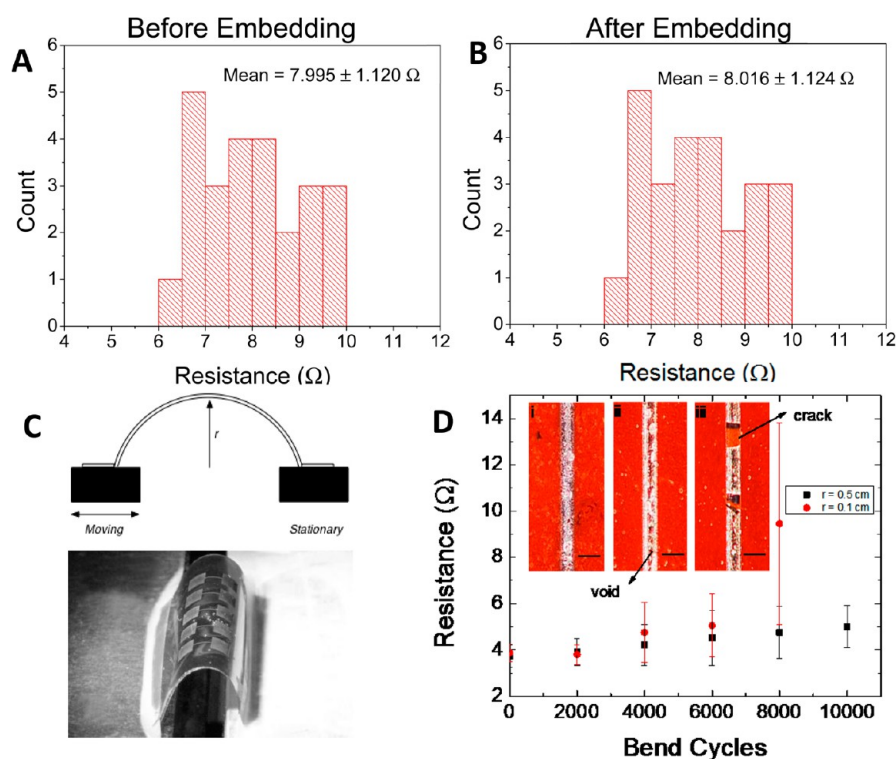
Figure 4. Histograms showing the distribution of electrical resistance of 25 silver lines (a) before and (b) after embedding. No significant change in the average resistance is observed. (c) Experimental setup for the bending test. The substrate, attached to a stationary block and a sliding stage, is bent to a certain radius and restored to its initial state at a rate of 10 cm s^{-1} to complete one bending cycle. (d) Electrical resistance of the embedded silver electrodes as a function of bending cycles under different bending radii (0.5 and 0.1 cm). Inset: Optical micrographs of embedded silver lines (i) before bend cycles and after (ii) 10 000 bending cycles for $r = 0.5$ cm and (iii) 8000 bending cycles for $r = 0.1$ cm. Scale bar is 50 μm.

custom-built bending test apparatus (Figure 4c), the substrate was bent to a certain radius and restored to its initial state at a rate of 10 cm s^{-1} to complete one bending cycle. As shown in Figure 4d, for r of 0.5 cm (~1.2% tensile strain), silver electrodes subjected to 10 000 repeated bending cycles exhibited only a slight increase (1.2-fold) in their electrical resistance relative to the initial value. Optical microscope images revealed a few voids in these electrodes that were not seen in the initial sample (Figure 4d i,ii). For r of 0.1 cm (6.2% strain), the electrical resistance increased gradually after many cycles, with a 2.4-fold increase after 8000 cycles. All the electrodes undergo cracking and failure after 10 000 cycles (Figure 4d iii). In ICD, because the embedded electrodes are flush with the top surface, they are subjected to the maximum strain in the multicomponent system upon bending. However, the bending performance of our embedded electrodes is not too different from as-printed silver electrodes reported in the literature[41] and should be acceptable for most flexible electronics applications. Further optimization of the bending performance may be possible by employing thinner electrodes but at the cost of reduced current carrying capacity. We also investigated the adhesion of the embedded metal tracks using the standard scotch tape peel test. The embedded electrodes remained intact and showed no visible protrusions even after three consecutive tests.

A special feature of ICD is the ability to fabricate embedded features in nonplanar surfaces. As a demonstration, we created wells with sloped sidewalls in a silicon wafer using conventional photolithography and wet-etching processes. Subsequently, the surface of this wafer was treated with a silane to make it low-energy (see Experimental Section). Silver lines were aerosol-jet

printed across a well in the wafer. The relatively large (2−5 mm) working distance in AJP enables uniform printing across the variable topography. Upon subjecting this substrate to ICD, a plateau in the epoxy coating is obtained with an embedded silver line running across it. Electrical measurements showed that the embedded silver line was conductive despite transcending an abrupt topography on the substrate. Scanning electron microscopy further confirmed a continuous transition of the embedded silver along the sloped part of the plateau (Supporting Information, Figure S5).

ICD should be promising for implementation in a continuous process employing printing and coating techniques. For example, high aspect ratio silver lines can be printed on a donor substrate using AJP or screen printing. The printed lines can be sintered rapidly with a flash sintering method.[42] Conventional industrial coating methods such as slot-die, curtain or roll coating can be used to apply a thin coating of a reactive polymer. In this work, we employed a thermally curable polymer, but a similar, fast-curing photocurable polymer should be equally effective.[43] The delamination step is performed routinely in continuous industrial processes, e.g. tape casting of ceramics.[44] Because of the reusability of the donor substrate, ICD may be performed in a continuous loop, thereby maintaining the benefits of additive manufacturing.

4. CONCLUSIONS

In conclusion, we have demonstrated a simple method for obtaining flexible substrates with embedded, printed silver lines. The unique ability of the aerosol jet to print on low energy surfaces enables successful transfer of printed features from a low energy donor substrate to a polymeric coating on a

receiving substrate. The polymer coating is strongly adhered to a supporting film, which lends mechanical robustness to the composite substrate and allows workability with thin coatings. The transfer yield is 100%, independent of size and orientation of the printed features or thickness of the coating. Importantly, surface roughness of the embedded electrodes is an order of magnitude lower than that of the as-printed electrodes. The embedded electrodes exhibit tremendous flexibility and resilience, not showing a significant degradation in electrical performance after thousands of bending cycles. Another attractive feature of ICD is the ability to create continuous embedded metal lines in nonplanar substrates. Because all constituting steps are additive and rapidly processable, ICD should be adaptable as an R2R manufacturing process.

■ ASSOCIATED CONTENT

Ⓢ Supporting Information

AFM height images of as-printed and embedded silver, s-PET, and epoxy coating; contact angle measurements of epoxy prepolymer liquid on s-PET and polyimide; optical image of embedded silver lines bent to a radius of 1 mm; optical micrograph of an embedded square grid and AFM height image of a crossover in the grid; cross-sectional SEM images of an embedded silver line across a topographical feature. This material is available free of charge via the Internet at http://pubs.acs.org.

■ AUTHOR INFORMATION

Corresponding Authors
*L. F. Francis. E-mail: lfrancis@umn.edu.
*C. D. Frisbie. E-mail: frisbie@umn.edu.
Notes
The authors declare no competing financial interest.

■ ACKNOWLEDGMENTS

■ REFERENCES

(1) Arias, A. C.; MacKenzie, J. D.; McCulloch, I.; Rivnay, J.; Salleo, A. Chem. Rev. 2010, 110, 3−24.
(2) Briand, D.; Oprea, A.; Courbat, J.; Bârsan, N. Mater. Today 2011, 14, 416−423.
(3) Tobjörk, D.; Österbacka, R. Adv. Mater. 2011, 23, 1935−1961.
(4) Lipomi, D. J.; Tee, B. C. K.; Vosgueritchian, M.; Bao, Z. Adv. Mater. 2011, 23, 1771−1775.
(5) Berggren, M.; Richter-Dahlfors, A. Adv. Mater. 2007, 19, 3201−3213.
(6) Nathan, A.; Ahnood, A.; Cole, M. T.; Sungsik, L.; Suzuki, Y.; Hiralal, P.; Bonaccorso, F.; Hasan, T.; Garcia-Gancedo, L.; Dyadyusha, A.; Haque, S.; Andrew, P.; Hofmann, S.; Moultrie, J.; Daping, C.; Flewitt, A. J.; Ferrari, A. C.; Kelly, M. J.; Robertson, J.; Amaratunga, G.; Milne, W. I. Proc. IEEE 2012, 100, 1486−1517.
(7) Khodagholy, D.; Doublet, T.; Gurfinkel, M.; Quilichini, P.; Ismailova, E.; Leleux, P.; Herve, T.; Sanaur, S.; Bernard, C.; Malliaras, G. G. Adv. Mater. 2011, 23, H268−H272.
(8) Khodagholy, D.; Doublet, T.; Quilichini, P.; Gurfinkel, M.; Leleux, P.; Ghestem, A.; Ismailova, E.; Hervé, T.; Sanaur, S.; Bernard, C.; Malliaras, G. G. Nat. Commun. 2013, 4, 1575.
(9) van Osch, T. H. J.; Perelaer, J.; de Laat, A. W. M.; Schubert, U. S. Adv. Mater. 2008, 20, 343−345.
(10) Sung, D.; de la Fuente Vornbrock, A.; Subramanian. IEEE Trans. Compon. Packag. Manuf. Technol. 2010, 33, 105−114.
(11) Meier, H.; Löffelmann, U.; Mager, D.; Smith, P. J.; Korvink, J. G. Phys. Status Solidi A 2009, 206, 1626−1630.
(12) Deganello, D.; Cherry, J. A.; Gethin, D. T.; Claypole, T. C. Thin Solid Films 2010, 518, 6113−6116.
(13) Stringer, J.; Derby, B. Langmuir 2010, 26, 10365−10372.
(14) Kang, H.; Kitsomboonloha, R.; Jang, J.; Subramanian, V. Adv. Mater. 2012, 24, 3065−3069.
(15) Mahajan, A.; Frisbie, C. D.; Francis, L. F. ACS Appl. Mater. Interfaces 2013, 5, 4856−4864.
(16) Fukuda, K.; Sekine, T.; Kumaki, D.; Tokito, S. ACS Appl. Mater. Interfaces 2013, 5, 3916−20.
(17) Chua, L.-L.; Ho, P. K. H.; Sirringhaus, H.; Friend, R. H. Appl. Phys. Lett. 2004, 84, 3400.
(18) Park, Y. D.; Kim, D. H.; Jang, Y.; Hwang, M.; Lim, J. A.; Cho, K. Appl. Phys. Lett. 2005, 87, 243509.
(19) Yoon, M.-H.; Yan, H.; Facchetti, A.; Marks, T. J. J. Am. Chem. Soc. 2005, 127, 10388−10395.
(20) Ortiz, R. P.; Facchetti, A.; Marks, T. J. Chem. Rev. 2009, 110, 205−239.
(21) Galagan, Y.; Rubingh, J.-E. J. M.; Andriessen, R.; Fan, C.-C.; Blom, P. W. M.; Veenstra, S. C.; Kroon, J. M. Sol. Energy Mater. Sol. Cells 2011, 95, 1339−1343.
(22) Galagan, Y.; Coenen, E. W. C.; Sabik, S.; Gorter, H. H.; Barink, M.; Veenstra, S. C.; Kroon, J. M.; Andriessen, R.; Blom, P. W. M. Sol. Energy Mater. Sol. Cells 2012, 104, 32−38.
(23) Galagan, Y.; Zimmermann, B.; Coenen, E. W. C.; Jørgensen, M.; Tanenbaum, D. M.; Krebs, F. C.; Gorter, H.; Sabik, S.; Slooff, L. H.; Veenstra, S. C.; Kroon, J. M.; Andriessen, R. Adv. Energy Mat. 2012, 2, 103−110.
(24) Yu, J. S.; Kim, I.; Kim, J. S.; Jo, J.; Larsen-Olsen, T. T.; Sondergaard, R. R.; Hosel, M.; Angmo, D.; Jorgensen, M.; Krebs, F. C. Nanoscale 2012, 4, 6032−40.
(25) Yu, J.-S.; Jung, G. H.; Jo, J.; Kim, J. S.; Kim, J. W.; Kwak, S.-W.; Lee, J.-L.; Kim, I.; Kim, D. Sol. Energy Mater. Sol. Cells 2013, 109, 142−147.
(26) Oh, S.; Yu, J.; Lim, J.; Jadhav, M.; Lee, T.; Kim, D.; Kim, C. IEEE Sens. J. 2013, 13, 3957−3961.
(27) Facchetti, A.; Yoon, M.-H.; Marks, T. J. J. Am. Chem. Soc. 2006, 128, 4928−4929.
(28) Hines, D. R.; Ballarotto, V. W.; Williams, E. D.; Shao, Y.; Solin, S. A. J. Appl. Phys. 2007, 101, 024503−9.
(29) Chen, J. H.; Ishigami, M.; Jang, C.; Hines, D. R.; Fuhrer, M. S.; Williams, E. D. Adv. Mater. 2007, 19, 3623−3627.
(30) Lee, D. Y.; Hines, D. R.; Stafford, C. M.; Soles, C. L.; Lin, E. K.; Oehrlein, G. S. Adv. Mater. 2009, 21, 2524−2529.
(31) Vogel, N.; Zieleniecki, J.; Koper, I. Nanoscale 2012, 4, 3820−3832.
(32) Liu, Y. F.; Feng, J.; Yin, D.; Bi, Y. G.; Song, J. F.; Chen, Q. D.; Sun, H. B. Opt. Lett. 2012, 37, 1796−1798.
(33) Yue-Feng, L.; Feng, J.; Cui, H.-F.; Yin, D.; Song, J.-F.; Chen, Q.-D.; Sun, H.-B. Appl. Phys. Lett. 2012, 101, 133303−133303−4.
(34) Zeng, X. Y.; Zhang, Q. K.; Yu, R. M.; Lu, C. Z. Adv. Mater. 2010, 22, 4484−8.
(35) Yu, Z.; Zhang, Q.; Li, L.; Chen, Q.; Niu, X.; Liu, J.; Pei, Q. Adv. Mater. 2011, 23, 664−668.
(36) Xu, F.; Zhu, Y. Adv. Mater. 2012, 24, 5117−5122.
(37) Liang, J.; Li, L.; Niu, X.; Yu, Z.; Pei, Q. Nat. Photonics 2013, 7, 817−824.
(38) Park, S.-I.; Ahn, J.-H.; Feng, X.; Wang, S.; Huang, Y.; Rogers, J. A. Adv. Funct. Mater. 2008, 18, 2673−2684.
(39) Sekitani, T.; Zschieschang, U.; Klauk, H.; Someya, T. Nat. Mat. 2010, 9, 1015−1022.

(40) Zheng, H.; Zheng, Y.; Liu, N.; Ai, N.; Wang, Q.; Wu, S.; Zhou, J.; Hu, D.; Yu, S.; Han, S.; Xu, W.; Luo, C.; Meng, Y.; Jiang, Z.; Chen, Y.; Li, D.; Huang, F.; Wang, J.; Peng, J.; Cao, Y. *Nat. Commun.*, **2013**, *4*, DOI: 10.1038/ncomms2971.

(41) Russo, A.; Ahn, B. Y.; Adams, J. J.; Duoss, E. B.; Bernhard, J. T.; Lewis, J. A. *Adv. Mater.* **2011**, *23*, 3426−30.

(42) Perelaer, J.; Schubert, U. S. *J. Mater. Res.* **2013**, *28*, 564−573.

(43) Ahn, S. H.; Guo, L. J. *Adv. Mater.* **2008**, *20*, 2044−2049.

(44) Mistler, R. E.; Twiname, E. R. *Tape Casting: Theory and Practice*, American Ceramic Society: Westerville, OH, 2000.

1312

dx.doi.org/10.1021/am405314s | *ACS Appl. Mater. Interfaces* 2014, 6, 1306−1312